Supporting Information

Unraveling Molecular Design Principle of Ferroelasticity in Organic Semiconductor Crystals with Two-Dimensional Brickwork Packing

Sang Kyu Park,[1,2↑*] Hong Sun,[3,4↑] Michael Bernhardt,[1] Kyoungtae Hwang,[2] John E. Anthony,[5] Kejie Zhao,[3*] Ying Diao[1*]

[1]Department of Chemical and Biomolecular Engineering, University of Illinois Urbana—Champaign, 600 S. Mathews Avenue, Urbana, Illinois 61801, United States.

[2]Functional Composite Materials Research Center, Institute of Advanced Composite Materials, Korea Institute of Science and Technology, 92 Chudong-ro, Bongdong-eup, Wanju-gun, Joellabuk-do, 55324, Republic of Korea.

[3]School of Mechanical Engineering, Purdue University, West Lafayette, Indiana 47907, United States.

[4]Physics Division, Lawrence Livermore National Laboratory, Livermore, California 94550, United States.

[5]Department of Chemistry & Center for Applied Energy Research, University of Kentucky, Lexington, Kentucky 40506-0055, United States.

*Correspondence to: yingdiao@illinois.edu, kjzhao@purdue.edu, skpark86@kist.re.kr

[↑]These authors contributed equally to this work

Table of Contents

Supporting Table

Table S1. Comparison of molecular packing parameters of 2D brickwork structures of TAS-acene molecules.

	π-π (a-b)[a]	π-π (a-c)[a]	Cg_{a-b}[b]	Cg_{a-c}[b]	Cg_{a-d}[b]	Cg_{a-e}[b]	θ_{pitch}[c]	θ_{yaw}[d]	θ_{roll}
TIPS-P	3.53 Å	3.20 Å	7.74 Å	10.19 Å	16.35 Å	16.96 Å	65.1°	1.1°	20.9°
TIPGe-P	3.51 Å	3.19 Å	7.76 Å	10.14 Å	16.33 Å	17.06 Å	64.3°	0.8°	20.3°
diF-TES-ADT	3.42 Å	3.26 Å	7.10 Å	8.46 Å	13.88 Å	17.16 Å	77.1°	20.3°	18.7°
diF-TIPS-ADT	3.37 Å	3.15 Å	8.10 Å	10.27 Å	16.95 Å	16.67 Å	60.7°	0.2°	17.3°

a: interplanar π-π distance. b: centroid-to-centroid distance. c: interplanar angle between molecular π-plane and (001). d: angle between molecular short axis and (001) plane normal. e: angle between (100) plane normal and (120) plane, angle between (010) plane normal and (210) plane, angle between (010) plane normal and (2-10) plane, and angle (100) plane normal and (-120) plane, for TIPS-P, TIPGe-P, diF-TES-ADT, and diF-TIPS-ADT, respectively. The molecular packing parameters are obtained from reported structure (TIPS-P: ccdc 1570910, TIPGe-P: ccdc 1889786, diF-TES-ADT: ccdc 691526, diF-TIPS-ADT: ref 1).

As depicted in **Fig. 2** all selected derivatives exhibit typical 2D brickwork packing. Along the main stacking (*a-b* pair) and the secondary stacking direction (*a-c* pair), π-π interactions occur that give rise to 2D electronic couplings in these crystals. Interplanar molecular distances in the *a-b* and *a-c* pairs are listed in the **Table S1**, showing 3.37–3.53 Å in the former and 3.15–3.26 Å in the latter pairs. The centroid-to-centroid (Cg-Cg) distances in *a-b* and *a-c* pairs are also examined (Cg_{a-b} and Cg_{a-c} **Table S1**), all showing shorter Cg_{a-b} distances than Cg_{a-c}. It is immediately noticeable that Cg_{a-b} : Cg_{a-c} ratios from the TIPS-P, TIPGe-P and diF-TIPS-ADT crystals are in the similar range (0.76–0.79) while it is much higher in the diF-TES-ADT case (0.84). We attribute appreciable change of this ratio in diF-TES-ADT to (i) geometric factor of the TES unit, and (ii) yaw angle (θ_{yaw}) tilting of the molecules in the structure (**Table S1** and **Fig. S9**, **S10**). As the TES unit has lower electron/spatial densities compared to TIPS or TIPGe unit and has T-shape geometry, neighboring TES units are able to come closer and stabilize the packing structure.[2] Alteration of θ_{yaw} is also ensued by TES substitution. The θ_{yaw} of diF-TES-ADT (20.3°), measured between molecular short axis and (001) plane normal (**Fig. S10b**), outliers significantly compared to the θ_{yaw} of the other molecules (0.2–1.1°). This not only allows closer Cg_{a-d} distance (**Fig. 2**) but also makes Cg_{a-c} distance shorter. In addition to the yaw angle tilting, pitch angle of the molecules (θ_{pitch}) slightly varies in these crystals, as summarized in **Table S1** and **Fig. S10a**. For TIPS-P and TIPGe-P crystals, θ_{pitch} is in a similar range of ca. 65°, while θ_{pitch} of diF-TES-ADT and diF-TIPS-ADT increased to 77.1° and decreased to 60.7°, respectively. Such structural factors (yaw and pitch angle tilting) greatly influence ferroelastic transformability of TAS-acene crystals by acene core / rotator side-chain interlocking.

Supporting Figures

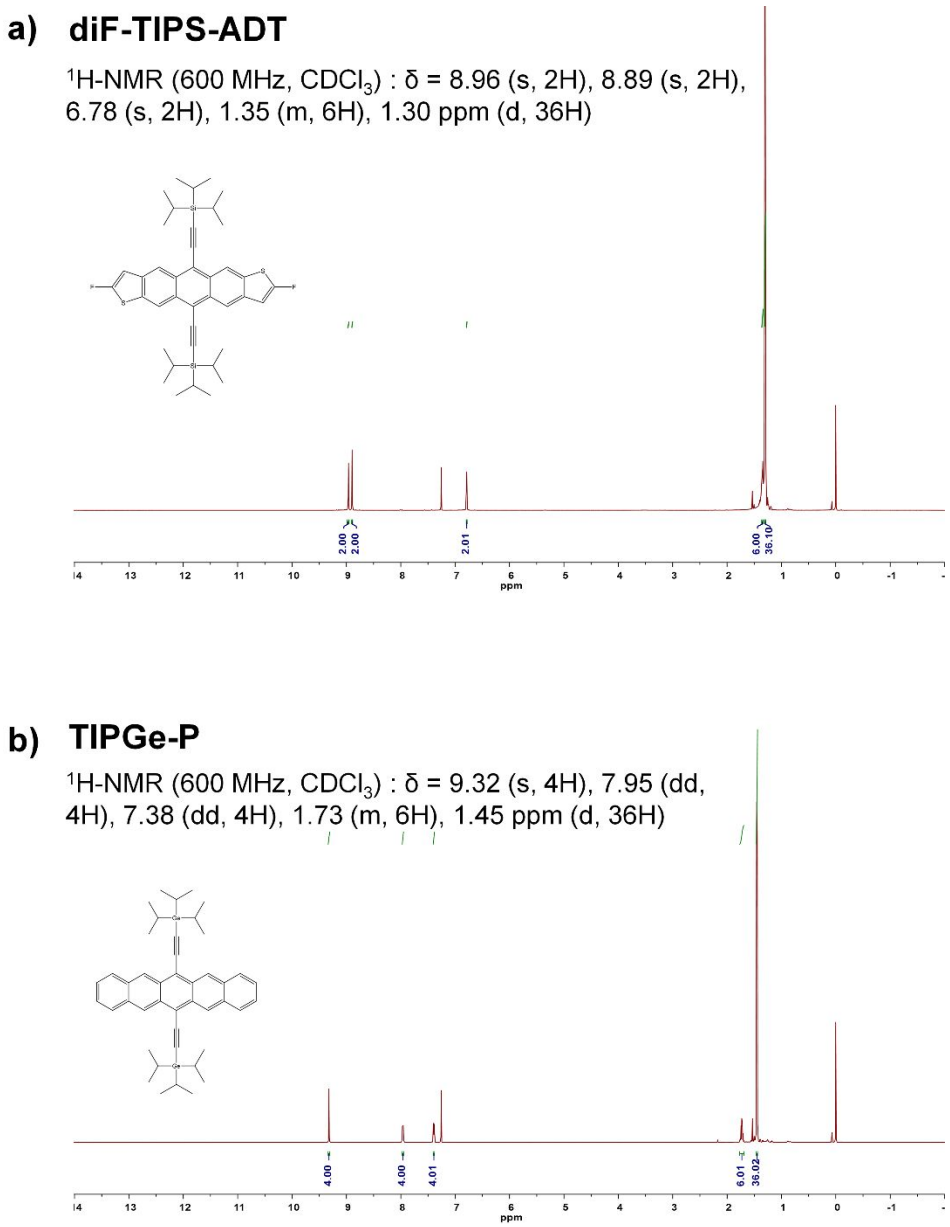

Fig. S1. 1H NMR spectra for a) diF-TIPS-ADT and b) TIPGe-P.

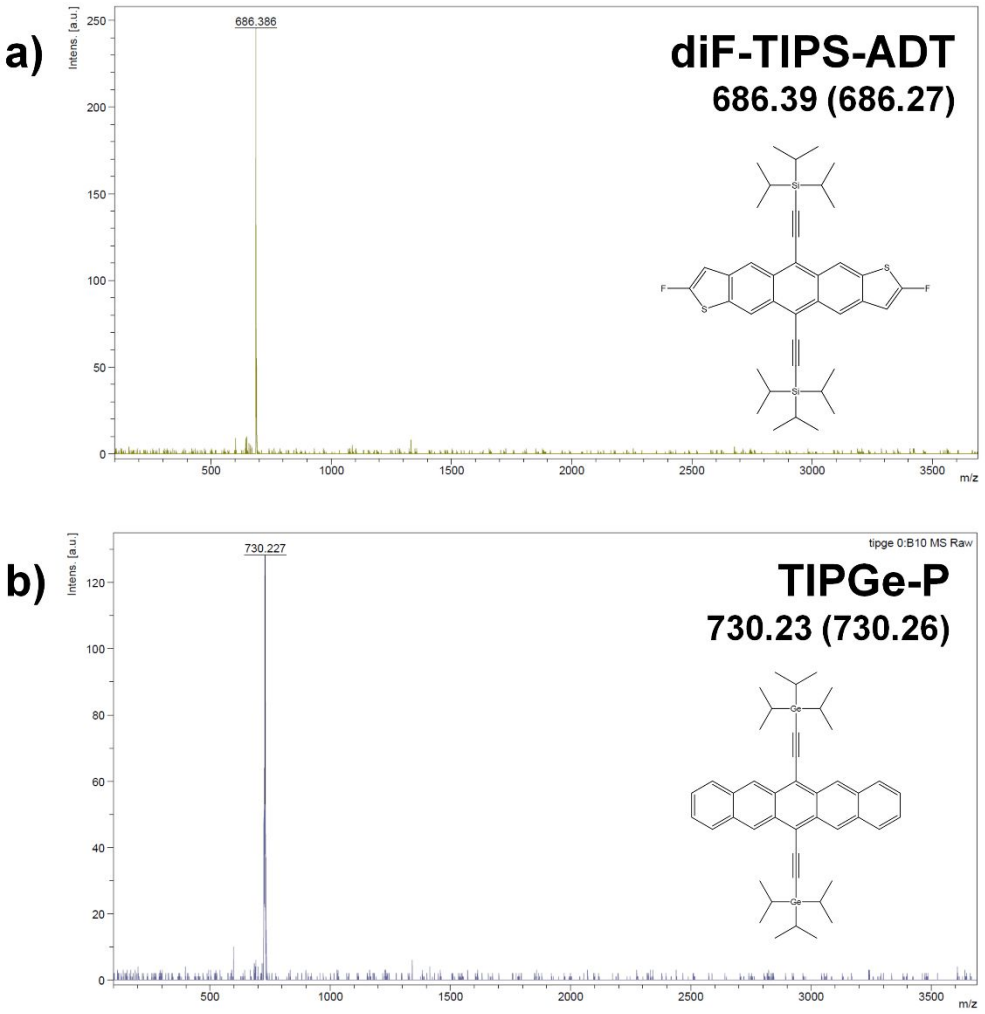

Fig. S2. Maldi-Tof spectra for a) diF-TIPS-ADT and b) TIPGe-P. MS (m/z) for diF-TIPS-ADT, Measured: 686.39, Calculated: 686.27. MS (m/z) for TIPGe-P, Measured: 730.23, Calculated: 730.26.

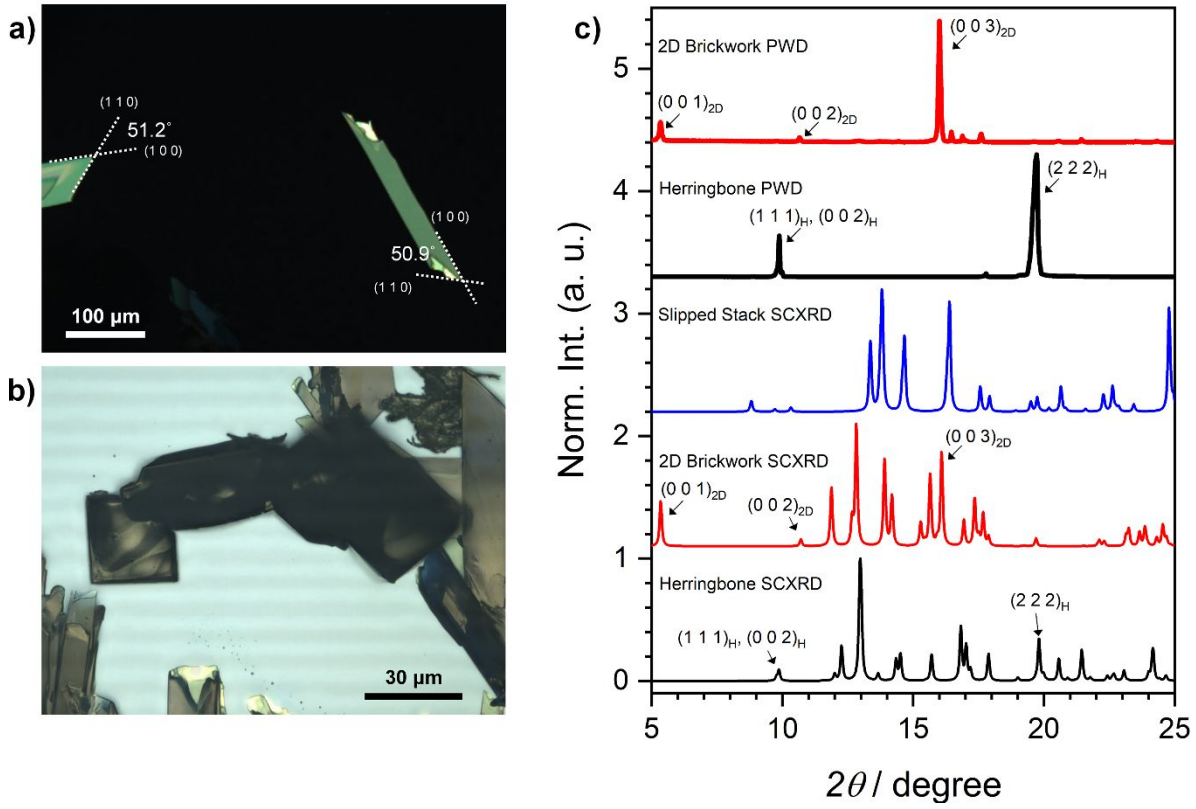

Fig. S3. Two major polymorphs (a: 2D-brickwork and b: herringbone packing crystals) produced by dropcasting TIPGe-P solution. a) As identified by SC-XRD in **Fig. S4**, ribbon tip of the 2D brickwork crystals exhibit specific angles of ca. 50˚, which correspond to the interplanar angle between (100) and (110) planes. b) The herringbone packing crystals, on the other hand, exhibit typical rectangular morphology of an orthorhombic structure. c) Powder X-ray diffraction patterns of the ribbon type and the rectangular crystals in comparison to SC-XRD results (ccdc: 1889786 – 1889788). The ribbon type crystals exhibit $(00n)$ peaks of 2D brickwork, while the rectangular crystals exhibit characteristic peaks (111), (002), and (222) of herringbone structure.

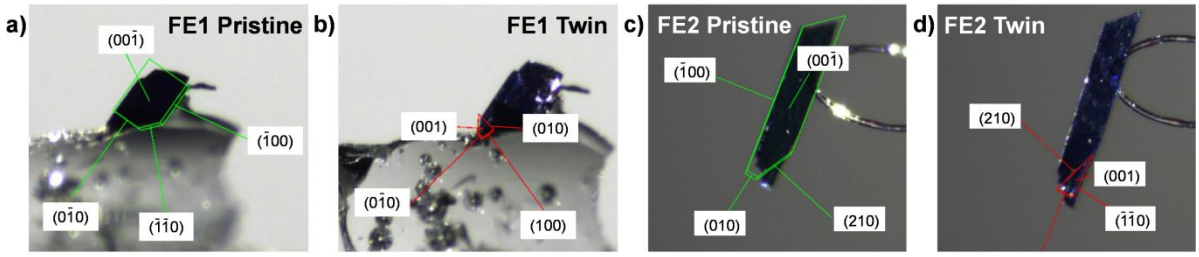

e)

	a	*b*	*c*	*α*	*β*	*γ*
FE1 Pristine	7.703	7.914	17.189	75.50	86.91	80.23
FE1 Twin	180°-Rotation about (010) plane normal, i.e., [-0.141 1 -0.094] with the twinning interface of $(010)_P/(0\text{-}10)_T$					
FE2 Pristine	7.704	7.889	16.928	78.16	88.95	80.74
FE2 Twin	180°-Rotation about [-120] with the twinning interface of $(210)_P/(210)_T$					

Fig. S4. Orientational relationships and indexed faces of twinned TIPGe-P crystal after FE1 and FE2 transitions. a) Indexed faces of the pristine domain and b) the twinned domain after FE1 transition. c) Indexed faces of the pristine domain and d) the twinned domain after FE2 transition. The faces are indexed using Bruker APEX 3 software. e) Table exhibits cell constants of the pristine domain of FE1 and FE2, and orientational relationship between the pristine and twinned domain after transition.

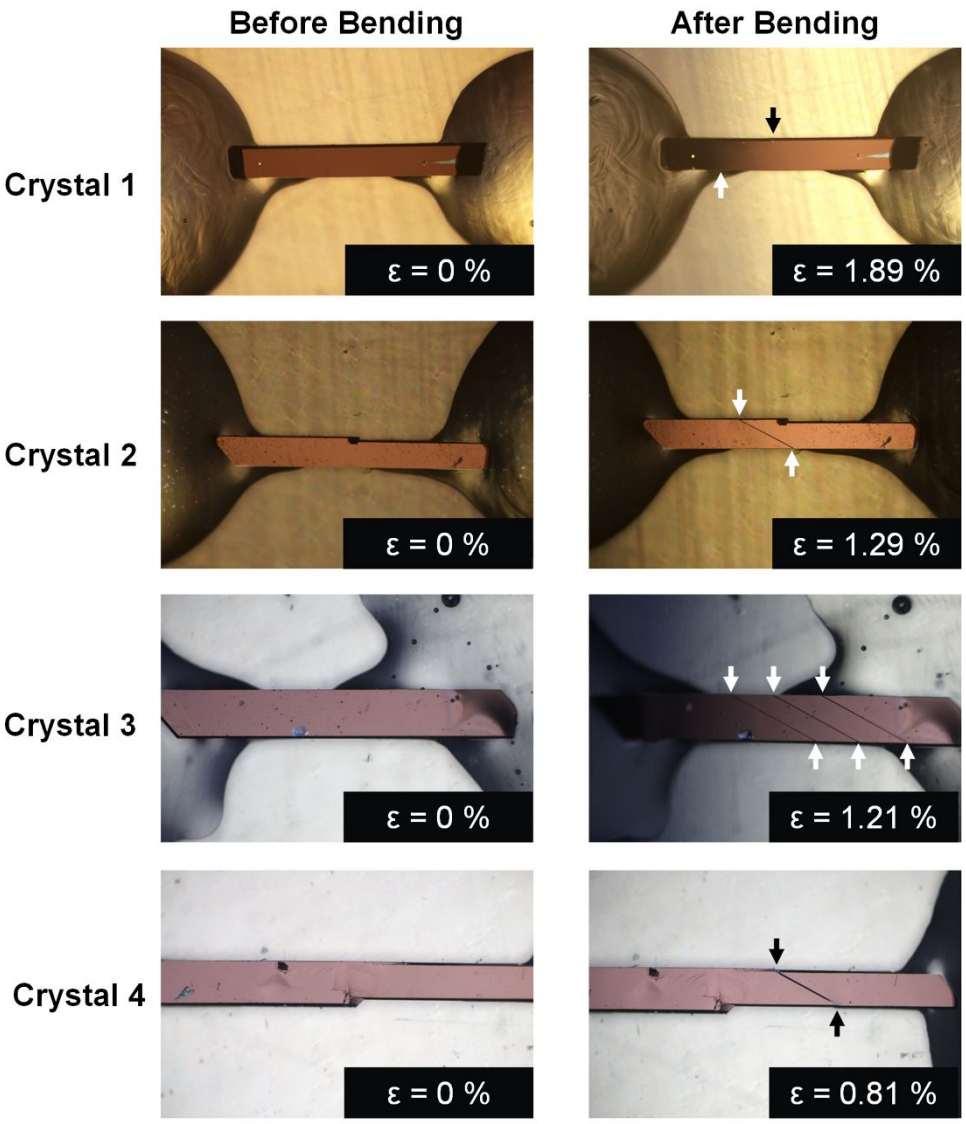

Fig. S5. Evaluated elastic limit for TIPS-P crystals under tensile loading. PET substrates with crystals attached are bent convexly to exert tension on the crystals under optical microscope. Tensile strain values in which thin twin domain(s) first appear are evaluated by $\varepsilon = t_{sub}/2r$, where ε is tensile strain, t_{sub} is thickness of the substrate (t_{sub} = 330 μm) and r is bending radius. Arrows in the micrographs indicate both ends of the twin domain(s).

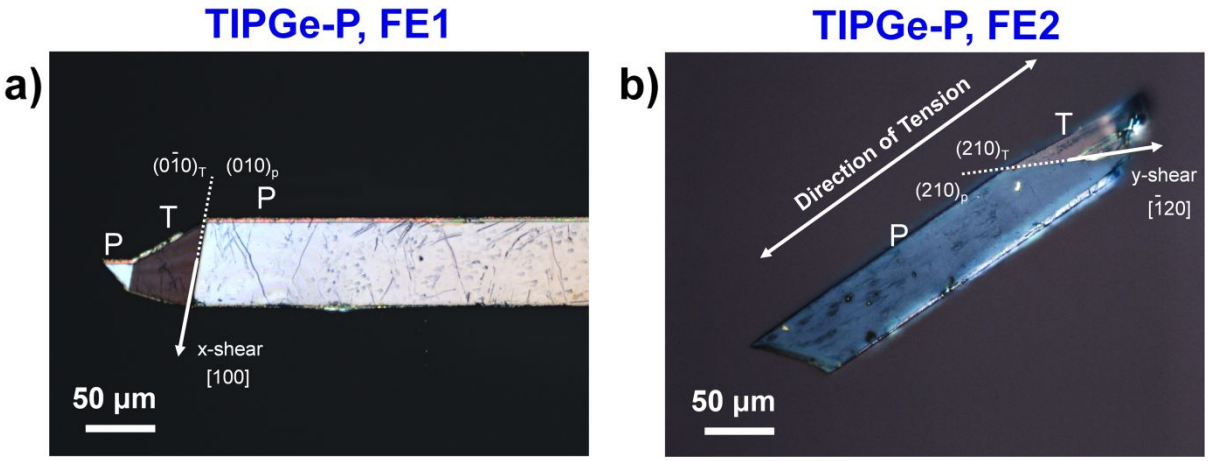

Fig. S6. Cross-polarized optical micrographic images of twinned TIPGe-P under a) x-shear and b) y-shear. The y-shear in b is accomplished by applying tension along the long axis of the crystals.

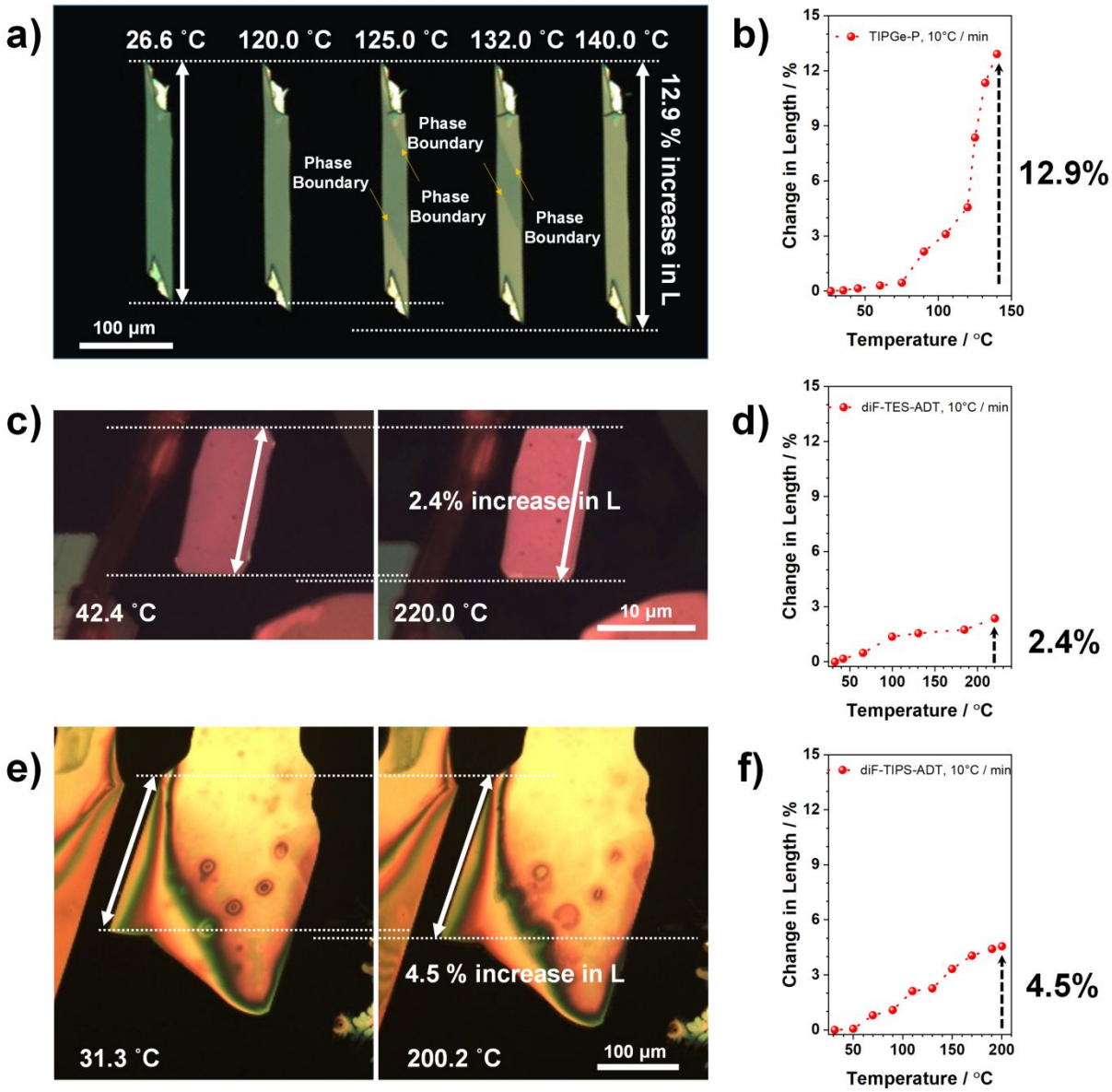

Fig. S7. Temperature-dependent length changes of a, b) TIPGe-P, c, d) diF-TES-ADT, and e, f) diF-TIPS-ADT crystals. Phase boundary sweeping is observed in TIPGe-P case due to the thermoelasticity, whereas diF-TES-ADT and diF-TIPS-ADT crystals do not exhibit such behavior.

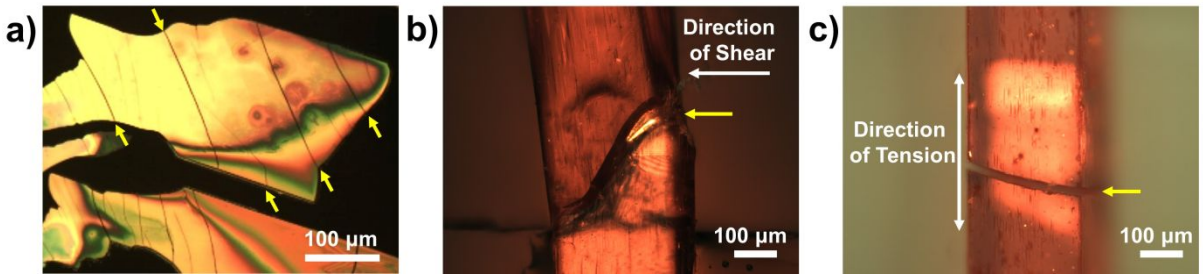

Fig. S8. Cross-polarized optical micrographic images of fractured crystals of diF-TIPS-ADT upon a) thermal annealing, b) direct x-shearing, and c) direct tensile loading. Cracks are indicated by yellow arrows. White arrows in b and c denote shear and tension directions, respectively.

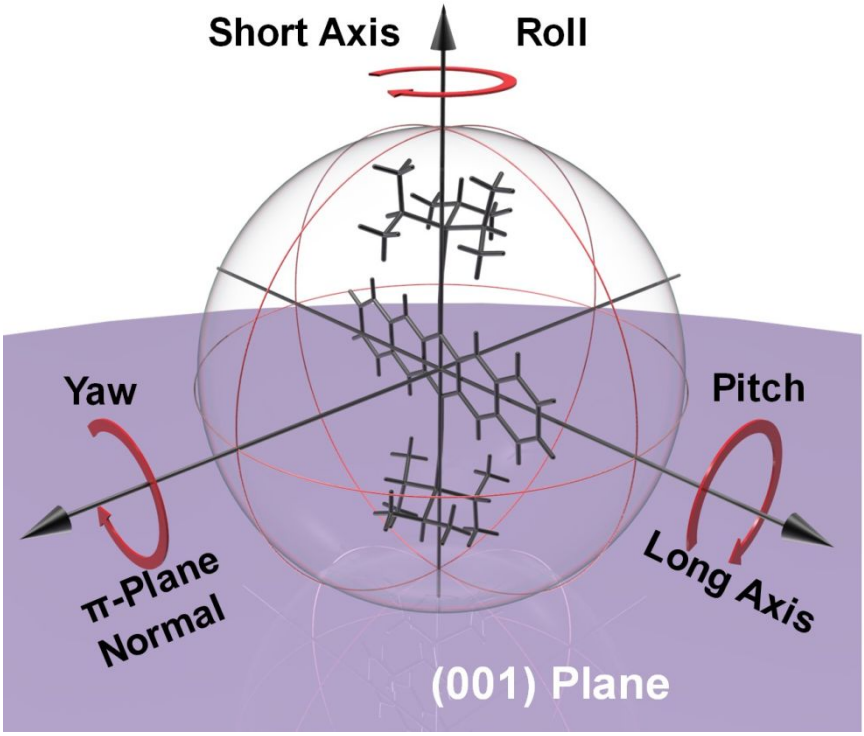

Fig. S9. Definition of pitch-yaw-roll angles. Pitch angle: angle between (001) and molecular π-plane. Yaw angle: angle between (001) plane normal and molecular short axis. Roll angle: angle between FE1 twin interface normal and molecular long axis; FE1 twin interfaces of TIPS-P, TIPGe-P, diF-TES-ADT, and diF-TIPS-ADT are (100), (010), (100), and (010), respectively. Note that molecule diF-TIPS-ADT does not show FE1 transition.

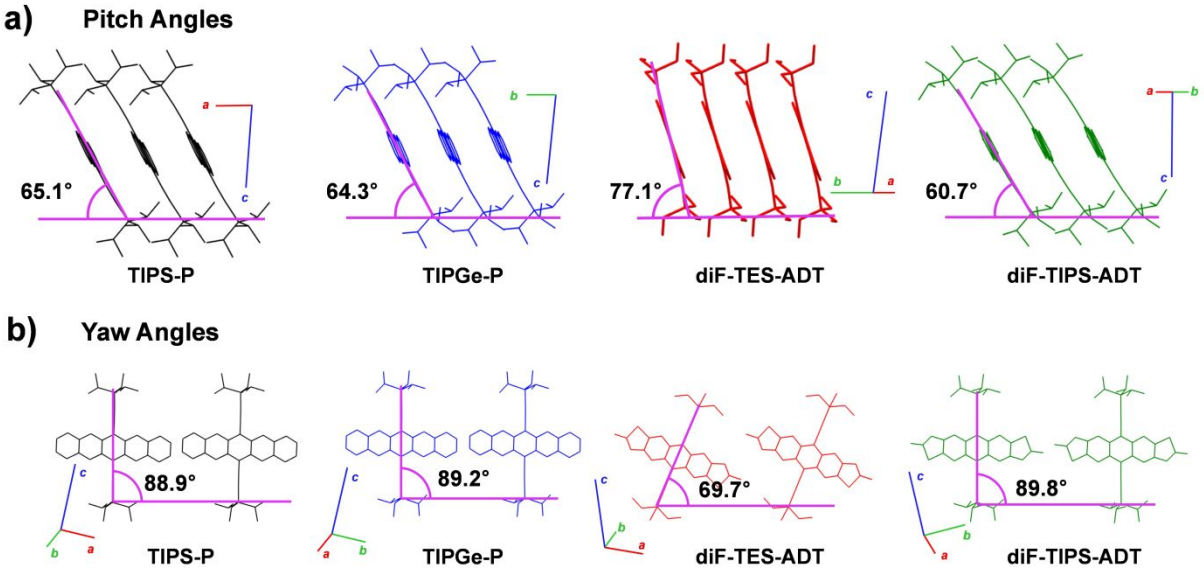

Fig. S10. a) Pitch angle and b) yaw angle views of the TAS-acene crystal structures. Pitch angles (θ_{pitch}) and counter yaw angles (90° – θ_{yaw}) measured in the crystal structures are indicated in a and b, respectively.

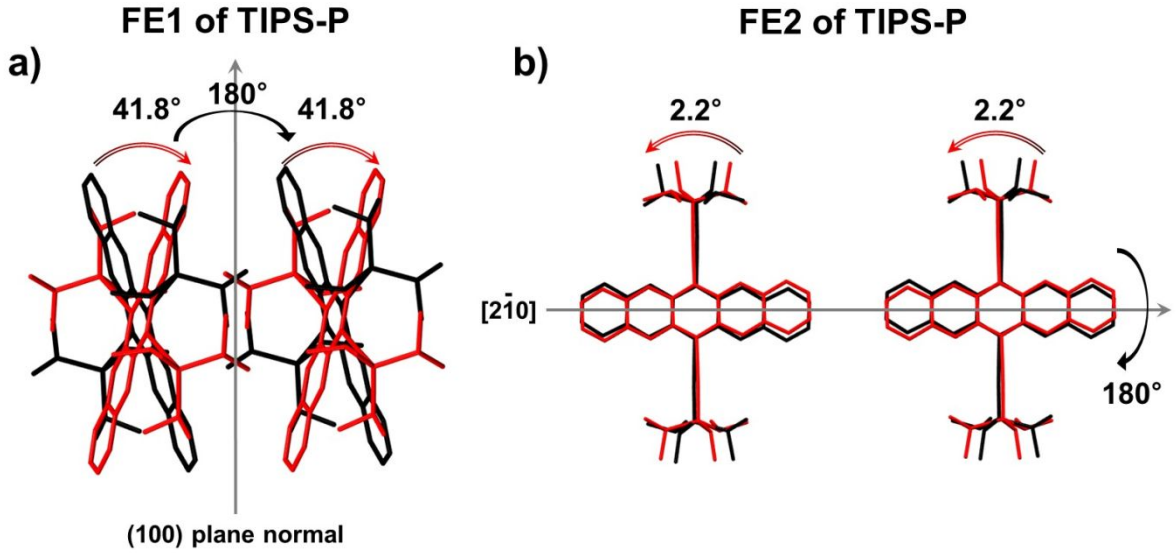

Fig. S11. a) FE1 transformation of TIPS-P based on 180°-rotation of the lattice around (100) plane normal (grey arrow). b) FE2 transformation of TIPS-P based on 180°-rotation of the lattice around $[2\bar{1}0]$ vector (grey arrow). The transformations result in 41.8° roll angle rotation and 2.2° yaw angle rotation of the molecules, respectively.

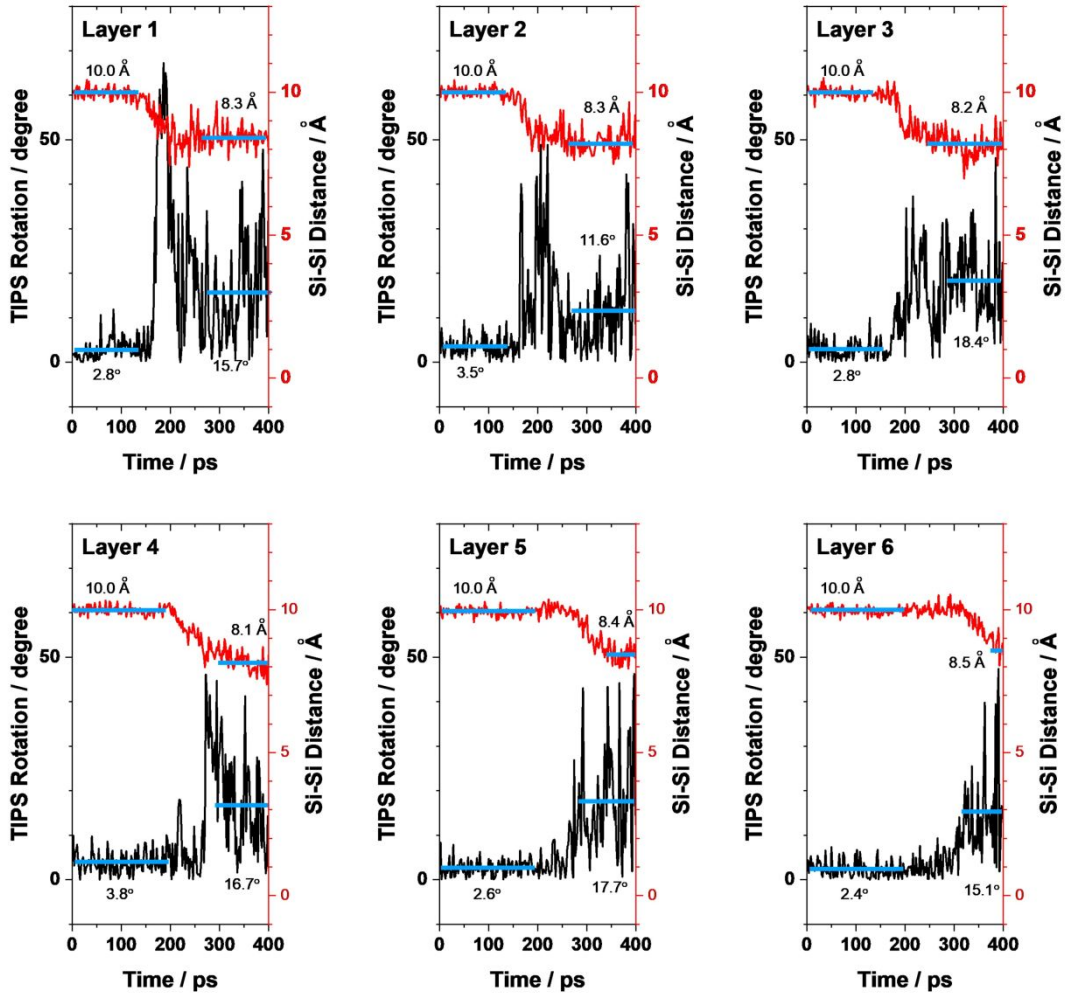

Fig. S12. Time dependent rotational angle of side-chain and Si-Si distance evolution plots of six different TIPS-P molecules in the adjacent molecular layers upon FE1 (**1-6** of **Fig. 3c**). The blue lines in each curve represents average of the rotational angle before and after FE1 transition. In the MD simulated FE1 process of TIPS-P, TIPS side-chains exhibit 12.9±2.7° rotation on average.

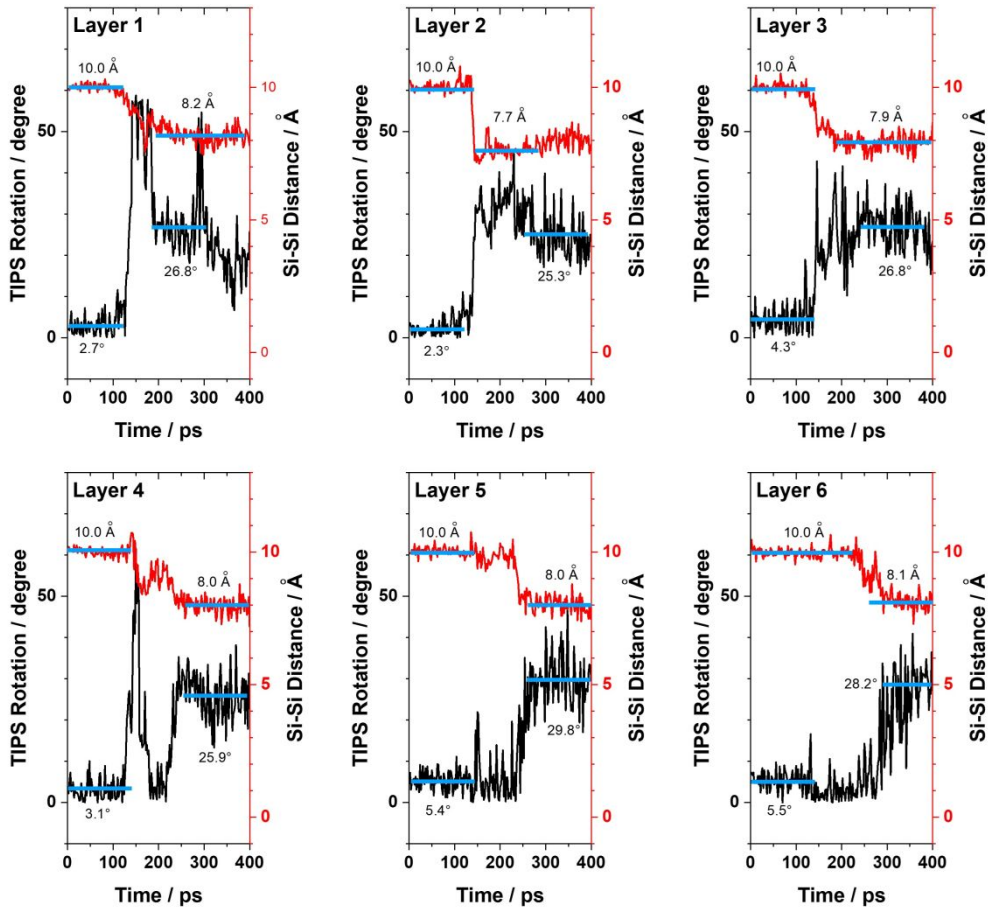

Fig. S13. Time dependent rotational angle of side-chain and Si-Si distance evolution plots of six different TIPS-P molecules in the adjacent molecular layers upon FE2 (**1-6** of **Fig. 3g**). The blue lines in each curve represents average of the rotational angle before and after FE2 transition. In the MD simulated FE2 process of **1**, TIPS side-chains exhibit 23.2±0.8° rotation on average.

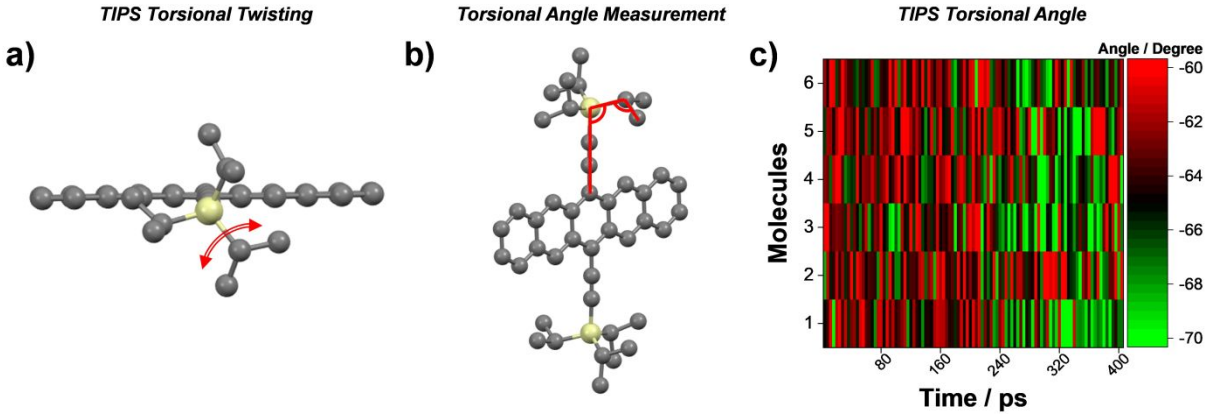

Fig. S14. a) MD simulated conformational changes of TIPS units. b) The torsional twisting angles of the propyl arms lying horizontally are characterized as marked in red lines. c) Conformational angle versus time contour plot of the propyl arms of TIPS units.

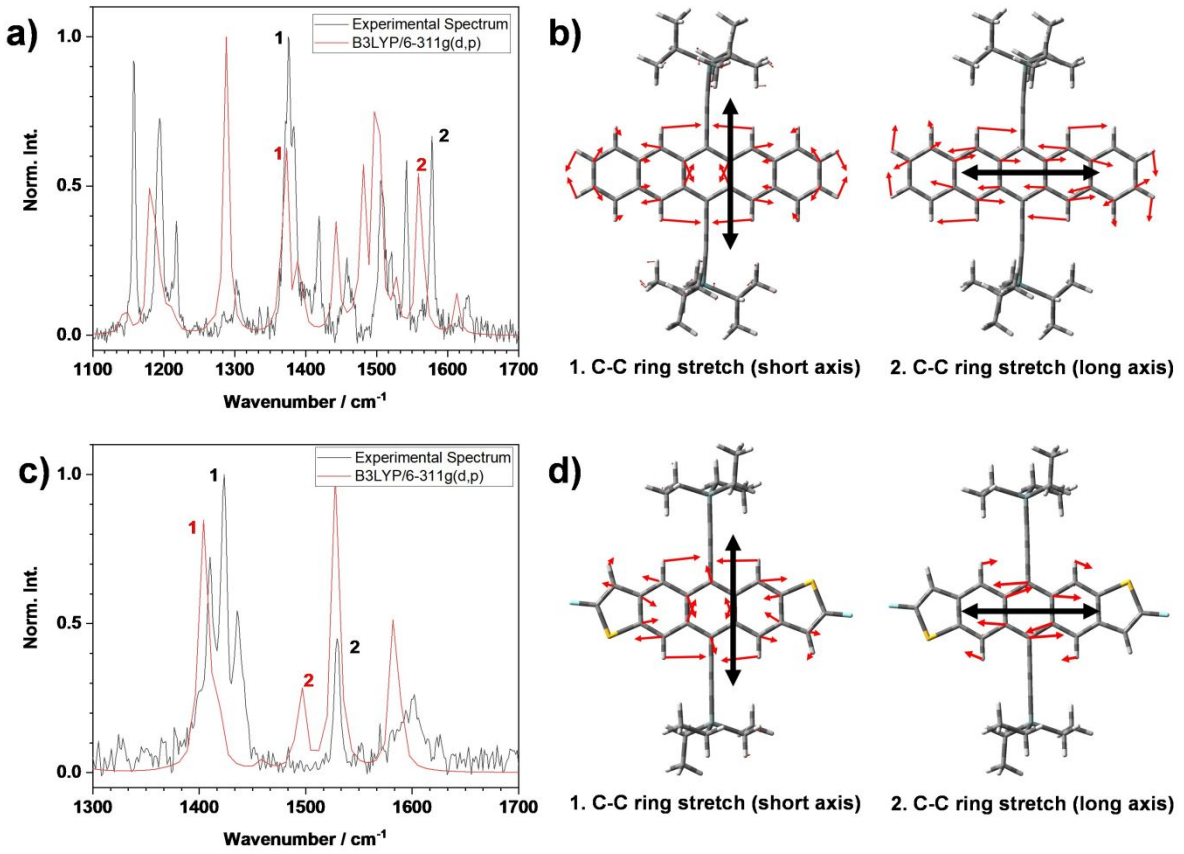

Fig. S15. Experimental (black) and DFT-calculated (red) Raman spectra of a) TIPGe-P and b) diF-TES-ADT, respectively. Intensity ratios between C-C stretching modes along short (1) and long axis (2), i.e., I_{1578} : I_{1375} and I_{1529} : I_{1421}, are investigated to verify acene core orientation of the twinned crystal of TIPGe-P and diF-TES-ADT, respectively. The polar plots of intensity ratios are represented in **Fig. 4d-f**. The wavenumbers of computational spectra are scaled by 0.967. c, d) Simulated atomic displacements for the Raman peaks 1 and 2 of TIPGe-P and diF-TES-ADT, respectively. Black arrows in c, d) denote the directions of polarization of vibration modes 1 and 2.

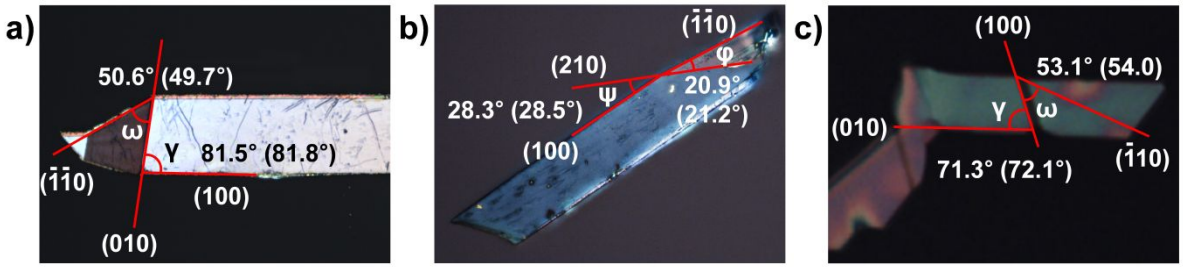

Fig. S16. Cross-polarized optical micrographic images of a) FE1 transformed TIPGe-P, b) FE2 transformed TIPGe-P, and c) FE1 transformed diF-TES-ADT crystals. By analyzing characteristic angles at the twin interface, we are able to assign side facet changes from (100) to $(\overline{1}\overline{1}0)$ for single crystals of TIPGe-P, and from (010) to $(\overline{1}10)$ for single crystals of diF-TES-ADT.

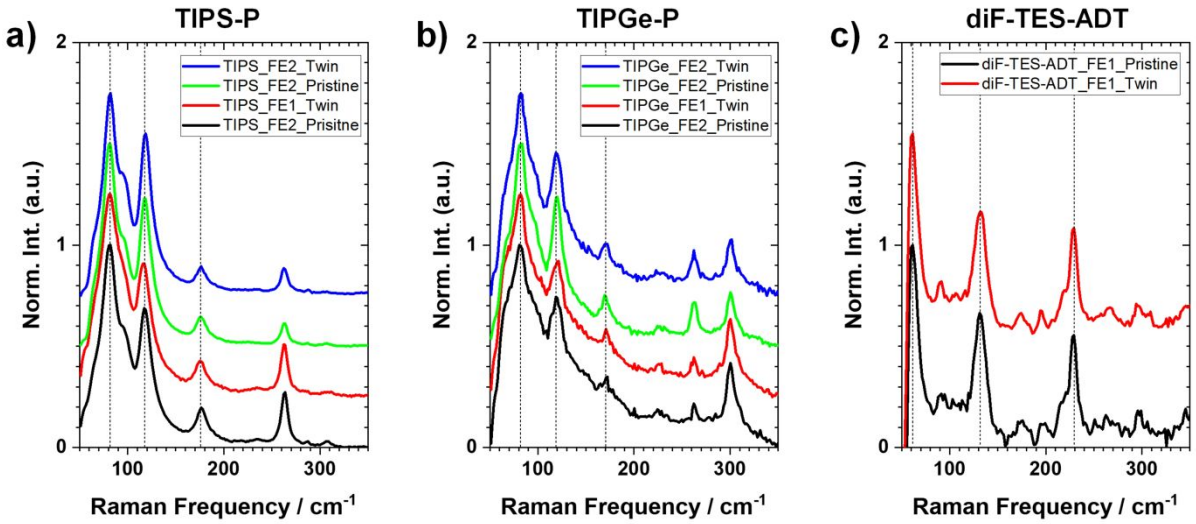

Fig. S17. Phonon vibration Raman spectra for a) TIPS-P, b) TIPGe-P, and c) diF-TES-ADT crystals. The peak frequencies before and after transition remain unchanged, which are suggestive of newly appeared domains are twins.

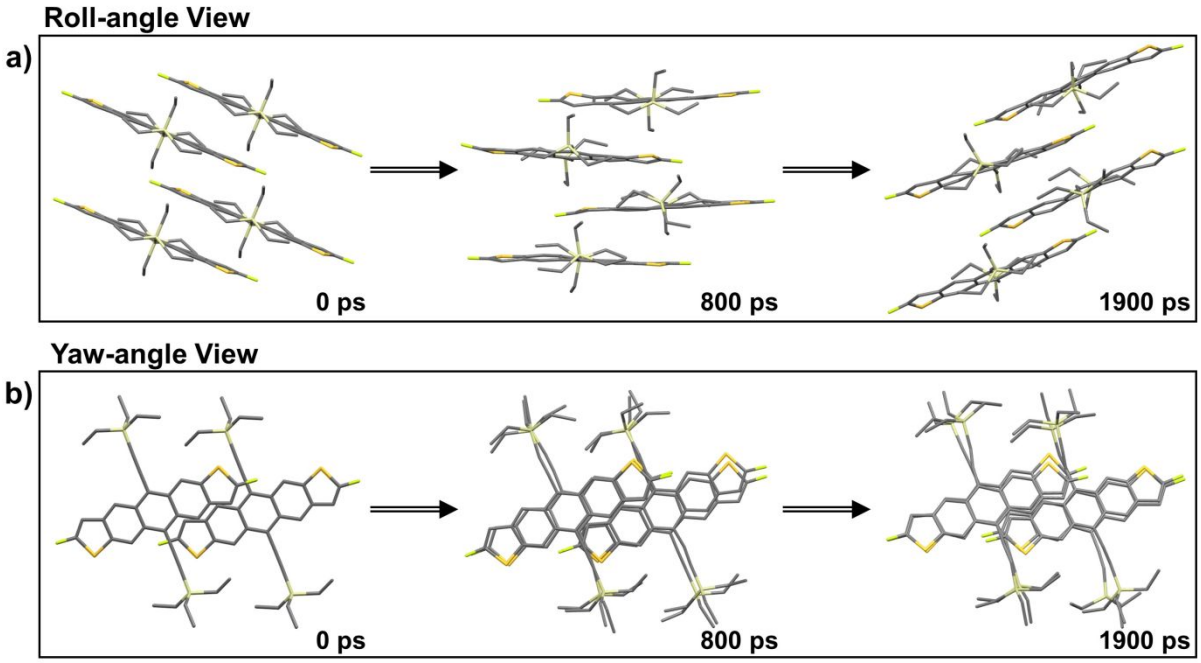

Fig. S18. AIMD modeling on FE1 of diF-TES-ADT structure viewed along a) the roll-angle and b) yaw-angle view. Modeled structure exhibits a consistent roll and yaw-angle in four different molecules, at the beginning, intermediate, and final shearing state.

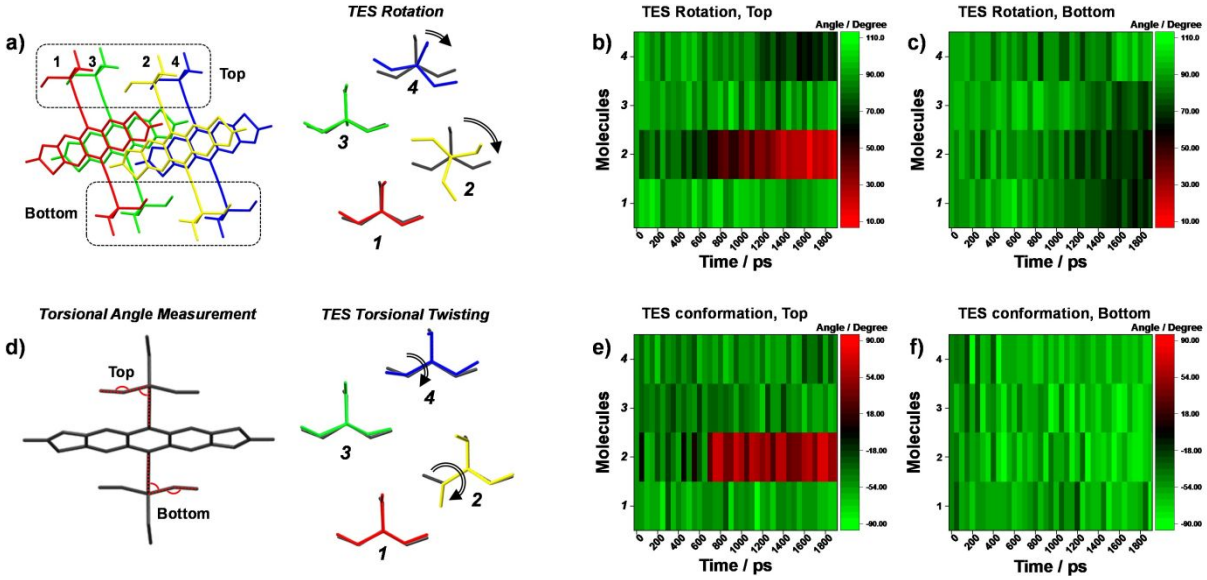

Fig. S19. a) AIMD simulated rotational motion of TES units, which are four at the top and four at the bottom. TES rotation angle versus time contour plot of TES units b) at the top and c) at the bottom. d) AIMD simulated conformational changes of TES units; the torsional twisting angles of the left ethyl arms are characterized as marked in the figure (red lines on the left). Conformational angle versus time contour plot of ethyl arms of TES units e) at the top and f) at the bottom.

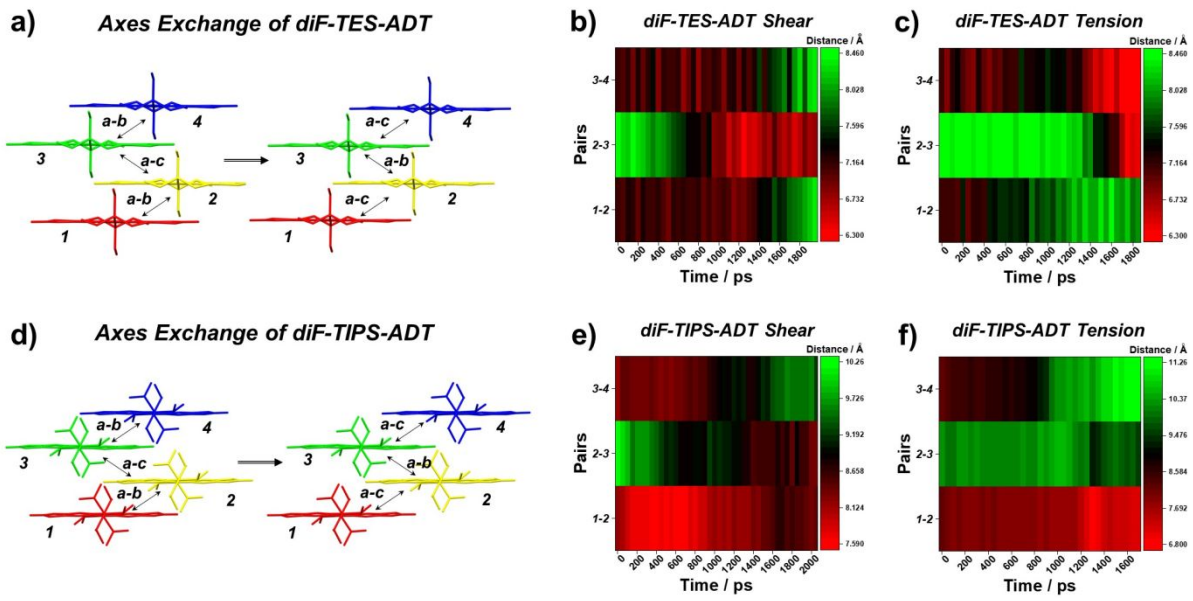

Fig. S20. a-c) Axes exchanging behavior of diF-TES-ADT. a) Structural representation, b) upon x-shear (FE1), and c) tensile loading. d-f) Axes exchanging behavior of diF-TIPS-ADT. d) Structural representation, e) upon x-shear (FE1), and f) tensile loading.

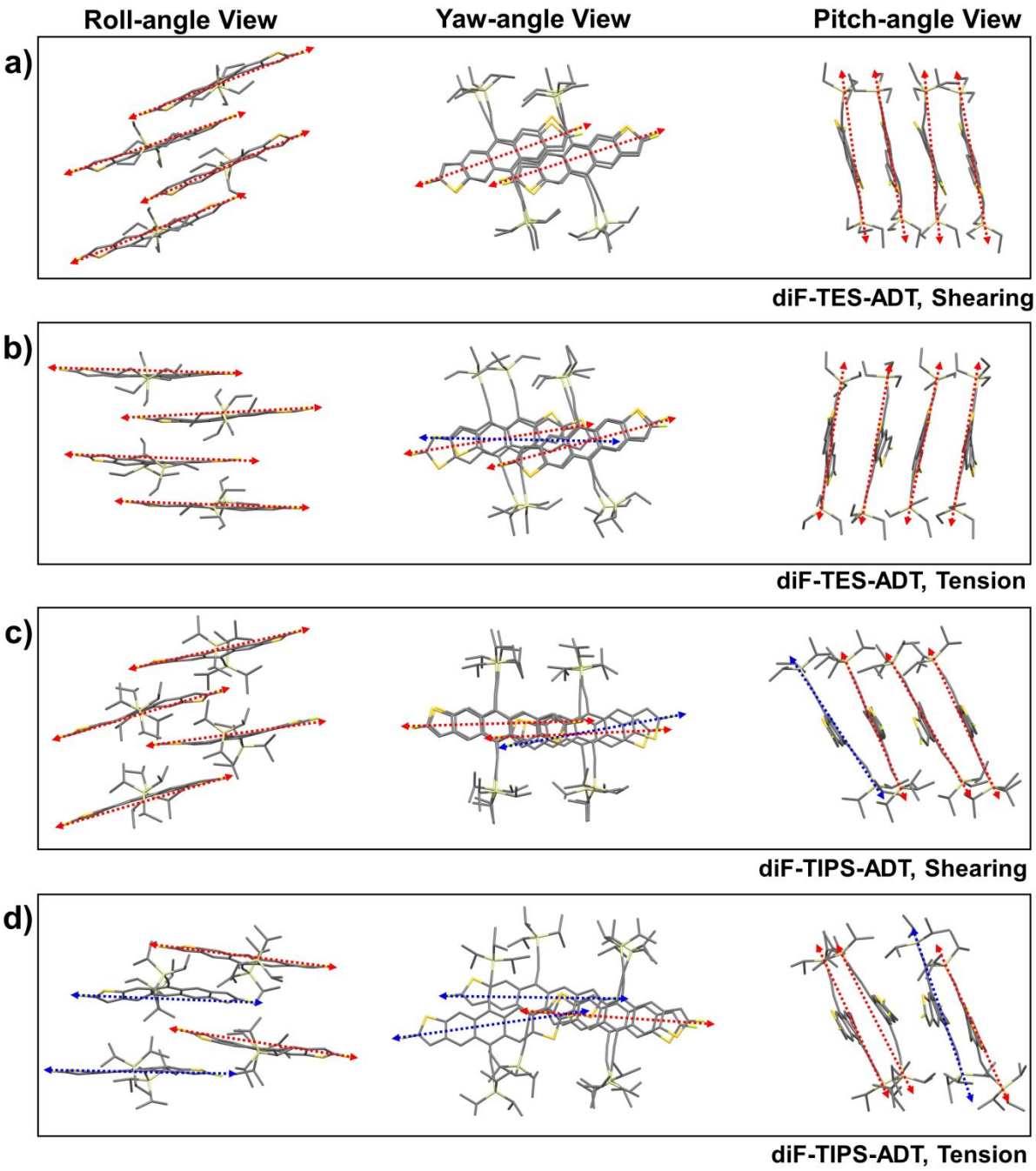

Fig. S21. Final state of a) x-sheared, b) tensioned diF-TES-ADT structure, c) x-sheared, and d) tensioned diF-TIPS-ADT structure, modeled by AIMD. Red dotted arrows represent molecular alignments with consistent pitch, yaw, and roll angles while blue dotted arrows represent molecular alignments with large deviations from the other molecules.

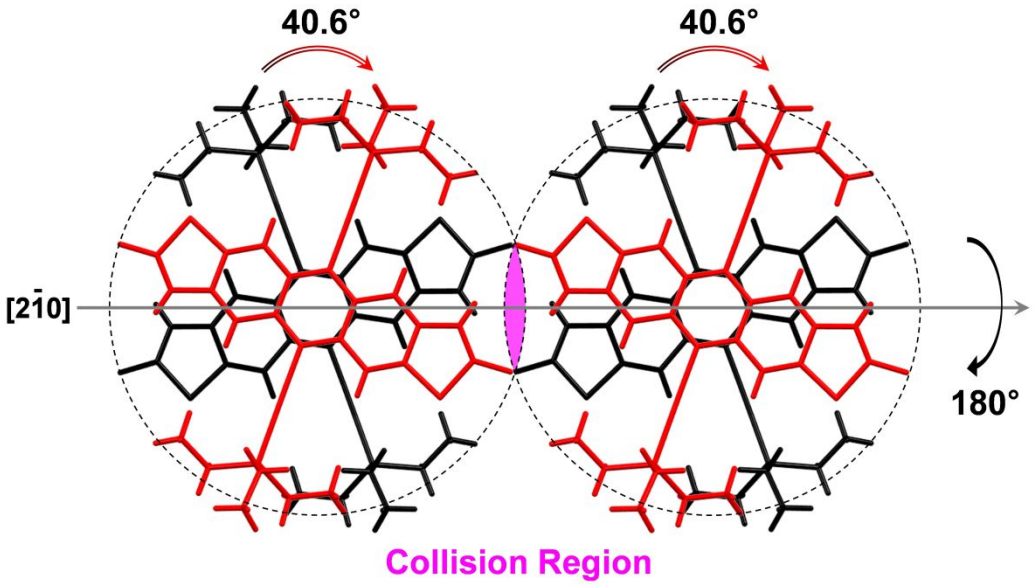

Fig. S22. Assumed molecular motion upon FE2 transition of the diF-TES-ADT structure. Due to the interdigitation of aromatic core units in the *a*-*d* pair, collision between the cores are expected, thus preventing such a transition.

Captions for Supporting Movies

Movie S1.

Thickness dependent adhesion of the TIPS-P crystals on the SiO_2/Si substrates at room temperature, evaluated by pushing crystals with Nylon wire.

Movie S2.

Thickness dependent adhesion of the TIPS-P crystals on the SiO_2/Si substrates at 150˚C temperature, evaluated by pushing crystals with Nylon wire.

Movie S3.

Thickness and adhesion dependence of ferroelastic transition based on thermal annealing.

Movie S4.

Thermal annealing induced thermoelasticity and subsequent cooling induced ferroelasticity of TIPGe-P crystal.

Movie S5.

Thermal annealing induced thermoelasticity and subsequent cooling induced ferroelasticity of TIPS-P crystal.

References

1. Subramanian, S.; Park, S. K.; Parkin, S. R.; Podzorov, V.; Jackson, T. N.; Anthony, J. E. Chromophore Fluorination Enhances Crystallization and Stability of Soluble Anthradithiophene Semiconductors. *J. Am. Chem. Soc.* **2008**, 130, 2706-2707.

2. Thorley, K. J.; Finn, T. W.; Jarolimek, K.; Anthony, J. E.; Risko, C. Theory-Driven Insight into the Crystal Packing of Trialkylsilylethynyl Pentacenes. *Chem. Mater.* **2017**, 29, 2502-2512.